Journal of Atmospheric and Solar-Terrestrial Physics 71 (2009) 88–100

Contents lists available at ScienceDirect

Journal of Atmospheric and Solar-Terrestrial Physics

journal homepage: www.elsevier.com/locate/jastp

Ionospheric response to the geomagnetic storm on 13–17 April 2006 in the West Pacific region

Biqiang Zhao [a,b,*], Weixing Wan [a], Libo Liu [a], K. Igarashi [c], K. Yumoto [d], Baiqi Ning [a]

[a] Institute of Geology and Geophysics, Chinese Academy of Sciences, Beitucheng West Road No. 19, Chaoyang District, Beijing 100029, China
[b] State Key Laboratory of Space Weather, Chinese Academy of Sciences, Beijing 100080, China
[c] National Institute of Information and Communications Technology, Tokyo, Japan
[d] Space Environment Research Center, Kyushu University, Japan

ARTICLE INFO

Article history:
Received 26 December 2007
Received in revised form
20 May 2008
Accepted 17 September 2008
Available online 17 October 2008

Keywords:
Magnetic storm
Total electron content
Mid-low latitude

ABSTRACT

This paper presents an investigation of geomagnetic storm effects in the equatorial and middle-low latitude F-region in the West Pacific sector during the intense geomagnetic storm on 13–17 April, 2006. The event, preceded by a minor storm, started at 2130 UT on April 13 while interplanetary magnetic field (IMF) B_z component was ready to turn southward. From 14–17 the ionosphere was characterized by a large scale enhancement in critical frequency, foF2 (4∼6 MHz) and total electron content (TEC) (∼30TECU, $1\text{TECU} = 1 \times 10^{16}\text{el/m}^2$) followed by a long-duration negative phase observed through the simultaneous ionospheric sounding measurements from 14 stations and GPS network along the meridian 120°E. A periodic wave structure, known as traveling ionospheric disturbances (TIDs) was observed in the morning sector during the initial phase of the storm which should be associated with the impulsive magnetospheric energy injection to the auroral. In the afternoon and nighttime, the positive phase should be caused by the combination of equatorward winds and disturbed electric fields verified through the equatorial F-layer peak height variation and modeled upward drift of Fejer and Scherliess [1997. Empirical models of storm time equatorial electric fields. Journal of Geophysical Research 102, 24,047–24,056]. It is shown that the large positive storm effect was more pronounced in the Southern Hemisphere during the morning-noon sector on April 15 and negative phase reached to lower magnetic latitudes in the Northern Hemisphere which may be related to the asymmetry of the thermospheric condition during the storm.

1. Introduction

Ionospheric storms remain a continuous fascinating and challenging topic of upper atmospheric physics since their discovery more than 70 years ago. During geomagnetic storms the magnetospheric energy input into the polar upper atmosphere can significantly modify the chemical and dynamics/electrodynamic processes of the ionosphere–thermosphere (I–T) system. Consequently, large disturbances in ionospheric electron densities and total electron content (TEC) are observed during geomagnetic storms (e.g. Mannucci et al., 2005). A number of excellent reviews have been published to summarize the current understanding of the ionospheric storm from both observations and theoretical models (e.g. Prölss, 1995; Schunk and Sojka, 1996; Abdu, 1997; Buonsanto, 1999; Danilov and Lastovička, 2001; Mendillo, 2006).

Now it is expected that the negative ionospheric storms in the high and middle latitude regions are induced by molecular composition bulge, which is created in the

* Corresponding author at: Institute of Geology and Geophysics, Chinese Academy of Sciences, Beitucheng West Road No. 19, Chaoyang District, Beijing 100029, China. Tel.: +86 10 82998310; fax: +86 10 82990846.
E-mail address: zbqjz@mail.iggcas.ac.cn (B. Zhao).

1364-6826/$ - see front matter © 2008 Elsevier Ltd. All rights reserved.
doi:10.1016/j.jastp.2008.09.029

auroral oval and then expands to lower latitudes by the horizontal neutral winds that arise from the pressure gradient force in the auroral oval and by ion drag in the polar cap (Fuller-Rowell et al., 1994, 1996). In the low latitude region, the ionospheric perturbations are produced by several processes. The heating of high latitude region launches equatorward wind surges that drag the low–-middle latitude plasma to higher altitudes along the magnetic field lines. An uplift of the plasma in that region induces an increase in plasma density owing to the decrease in molecular gases (or decrease in O^+ loss rate) at higher altitudes. The increase in NmF2 following an increase in hmF2 and its time delay at lower latitudes was provided as evidence of traveling atmospheric disturbances (TADs) that drive positive ionospheric storms in the low and middle latitudes (Prölss, 1993). On the other hand, model simulations showed that the divergence and upwelling of the polar upper atmosphere during a storm could set up a Hadley-type circulation cell that produces its convergence and downwelling in the low and middle latitudes. The downwelling of the atmosphere causes a decrease in molecular gases in the thermosphere, leading to a decrease of recombination rate of O^+, and then induce a positive storm effect (e.g. Rishbeth et al., 1987; Burns et al., 1995; Meier et al., 2005). However, recent study by Immel et al. (2001) indicated both processes, uplift of the ionosphere and thermospheric composition change, could occur simultaneously. Their observations showed that the perturbed hmF2 measured from ionosonde network and the enhanced O I 130.4-nm emission obtained from DE 1 data propagate in phase from high to lower latitudes, which was also identified from their model simulations using the thermosphere/ionosphere/mesosphere electrodynamics general circulation model (TIMEGCM). Another important factor that influences the storm-time behavior of the low latitude ionosphere is the electric fields. Under the effects of the prompt penetration electric fields and the wind disturbance dynamo electric fields, equatorial ionization anomaly (EIA) can undergo a drastic modification resulting in large ionospheric disturbances at low latitude (e.g. Abdu et al., 1991). Normally during a magnetic storm, several mechanisms work together to produce the observed storm effects and their relative importance differs from case to case and phase to phase of the storm. Recently, by using the Coupled Magnetosphere Ionosphere Thermosphere (CMIT) 2.0 model, Lei et al. (2008a) have successfully reproduced the significant positive storm effects occurred in the Atlantic sector after the onset of the December 2006 magnetic storm. Further, the authors introduce a term analysis for the continuity equation to investigate the relative importance of the winds, electric fields and composition in explaining the large-scale storm effects.

In spite of a large number of case studies and sophisticated modeling, there are still open questions and contradictions in understanding of some aspects of ionospheric storms (Burns et al., 2007). Thus case study of the ionospheric storm is still valuable in providing detailed information of ionospheric disturbances under different season, location, solar activity. In the maximum and descending phase of the 23th solar cycle, there occurred a number of large magnetic storms, which induced profound changes at a global scale. In the East-Asian/Australian region, ionospheric disturbances during these magnetic storms have been investigated observationally and theoretically (e.g. Lee et al., 2004; Liu et al., 2004; Lynn et al., 2004; Kane, 2005; Kutiev et al., 2005; Zhao et al., 2005, 2007; Maruyama and Nakamura, 2007; Yizengaw et al., 2005; Pirog et al., 2006, 2007). For most studies, the ionospheric storm was produced by a coronal mass ejection (CME) while in our present case, ionospheric storm was triggered by the solar wind high-speed stream under low solar activity. Based on a chain of ionosondes and GPS network, we will show that the ionospheric response was rather drastic with some of its features, for example the large positive storm effect superposed with periodic wave structures, resembling that occurred during the superstorm on 7–10 November 2004 (Pirog et al., 2007; Lekshmi et al., 2008). We will discuss the electrodynamic process and thermospheric response of the storm and hoping that it would be helpful to other scientists, who analyze the same storm for the other geographic region.

Table 1
Information of ionosonde station.

Station		Geographic latitude (deg)	Geographic longitude (deg)	Geomagnetic latitude (deg)	Dip (deg)	Resolution (min)
Code	Name					
WK	Wakkanai	45.3	141.6	35.3	59.1	60
BJ	Beijing	40.3	116.2	29.6	58.8	5
OS	Osan AB	37.1	127.0	27.3	53.5	15
KO	Kokubunji	35.6	139.5	25.5	49.6	60
YA	Yamagawa	31.2	130.6	20.4	44.1	60
OK	Okinawa	26.3	127.8	15.3	36.8	60
CL	Chung-li	25.0	121.2	15.0	36.2	15
HA	Hainan	19.4	109.0	8.1	26.8	15
KW	Kwajalein	9.0	167.2	3.3	8.0	5
VA	Vanimo	−2.7	141.3	−12.6	−22.1	60
DW	Darwin	−12.5	131.0	−22.4	−41.2	60
LM	Learmonth	−21.8	114.1	−32.5	−56.2	15
MU	Mundaring	−32.0	116.4	−42.6	−67.0	60
CA	Camdan	−34.0	150.7	−44.0	−66.3	60
HO	Hobart	−42.9	147.3	−51.7	−72.9	60

2. Data source

The quarter hourly ionosonde data used in the present study were provided from Institute of Geology and Geophysics of Chinese Academy of Sciences (IGGCAS), websites of National Institute of Information and Communications Technology of Japan, Ionospheric Prediction Service of Australia, Space Physics Interactive Data Resource and Digital Ionosonde Data Base at Lowell University of United States. The information of all stations is listed in Table 1. Most stations cover the longitudinal range 114–150°E with local time difference of 2 h and latitudinal range from −43° to 45°N. The equatorial station Kwajalein (KW) is the most eastward station with longitude about 167°E. Considering the ionospheric storm is a large-scale effect, this longitude difference is allowable. During the daytime, since the Cowling effect associated with the equatorial electrojet (EEJ) has an amplify function on the equatorial east–west electric field, the difference component of the horizontal (H) component between a magnetometer placed directly on the magnetic equator and one displaced 6–9° away can be used to derive the vertical $E \times B$ drift in the equatorial F-region (Anderson et al., 2002). Here we use the H component of the ground magnetometers at Muntinlupa (MUT) and Cebu (CEB), whose geomagnetic latitudes are 2.5°N and 6.8°N, to present disturbed electric fields information during the daytime. The two magnetometers are located near geographic longitude 120°E and belong to the project of MAGnetic Data Acquisition System (MAGDAS), which is constructed by Space Environment Research Center (SERC), Kyushu University (Yumoto and the MAGDAS Group, 2006).

The GPS data are from the International Global Navigation Satellite System Service (IGS) GPS tracking network covering around East-Asian/Australian sector. Around 70 GPS receivers are used to derive the grid TEC value at longitude 120°E. Using least-square fit and nearest-neighbor interpolation method slant TEC observations are converted to vertical TEC data of 2.5° grid. The details of this algorithm were described by Mao et al. (2008). To discuss changes in the thermospheric composition, we have used experimental data of the daytime O/N_2 column density obtained by the GUVI instrument on board the TIMED satellite. The GUVI column O/N_2 ratio is determined from the O (135.6 nm) and N_2 (LBH) emissions (Christensen, 2003; Paxton, 2004; Strickland et al., 2004) and is estimated with $1.75° \times 1.75°$ spatial resolution. Solar wind parameters and geomagnetic indices were obtained from Coordinated Data Analysis Web and World Data Center, Kyoto.

3. Solar wind and geophysical condition

The solar activity was low to moderate during April 2006. The mean 10.7 cm solar radio flux index $F_{10.7}$ was 89. No partly or fully Earth directed CMEs were observed in LASCO imagery. Under the influence of a strong high-speed stream from a recurrent trans-equatorial coronal hole (CH220), the earth's geomagnetic field was active to severe storm on 14 April (http://www.dxlc.com/solar/old_reports/). Fig. 1 illustrates the solar wind and interplanetary environment parameters and geomagnetic disturbance indices during the period 13–17 April 2006. Fig. 1 shows, from above to bottom, the solar wind velocity V_{sw}, solar wind dynamic pressure P_{dyn}, Z component of interplanetary magnetic field (IMF) B_z in the GSM coordinate measured from ACE satellite, AE, Kp and Dst indices. As shown in Fig. 1, solar wind speed was between 400 and 700 km/s during this event and started to increase at ~0800 UT on 13 April, while P_{dyn} showed a large increase from 1.6 to 12 nPa afterward. B_z turned southward at 0500 UT and became fluctuated and kept stable northward at 1500 UT. Kp reached 4, Dst decreased to −43 nT and AE reached 740 nT during this period indicating geomagnetic condition was already disturbed on 13 April. After 2130 UT on 13 April the northward IMF B_z started to decrease and became stable southward with a magnitude of 15 nT, which triggered a large but gradual Dst decrease (−122 nT) on 14 April. Kp reached 7 and AE increased to 1860 nT during the main phase of magnetic storm suggesting that magnetosphere–ionosphere coupling process was intense. The recovery phase of the storm was rather long which presented a second decrease of Dst on 15 April. Our study mainly focuses on the first decreasing stage since the ionospheric effect during this period was much more significant than during the latter. The solar flux $F_{10.7}$ during the period ranged from 77 to 81.

4. Results and analysis

4.1. General feature

Figs. 2a and b show plots of foF2 observed by 12 ionosonde stations in the East-Asian/Australian sector during the period of 13–17 April 2006. Monthly median values are also presented for comparison. The Dst index for the 5-day period is also shown for comparison with the ionosonde data. As shown in Fig. 2a, during the main phase of the storm on 14 April, the foF2 experienced a large enhancement from middle latitude station WK (geomagnetic latitude: 35.3°N) to low atitude station OK (15.3°N). Furthermore, this positive phase is clearly characterized by a wave structure. Following the positive storm effect is the lasting negative storm effect that appeared first at station WK (35.3°N) around 1500 UT on 14 April and persisted until the end of 16 April. At low latitude station YA (20.4°N) and OK (15.3°N), foF2 showed a decrease after 0600 UT on 15 and 16 April. At station HA (8.1°N), foF2 changed little compared with the higher latitude stations.

In the Australian region, foF2 displayed a similar evolvement with a positive phase and then followed by a long-lasting negative phase in the middle latitude as shown at HO (51.7°S) and CA (44.0°S). However, there is clear difference in the ionospheric response between the two hemispheres. Negative storm effect appeared first at WK (35.3°N) around 1500 UT while at MU (42.6°S) around 2000 UT on 14 April. Negative phase penetrated into lower geomagnetic latitude in the Northern Hemisphere as

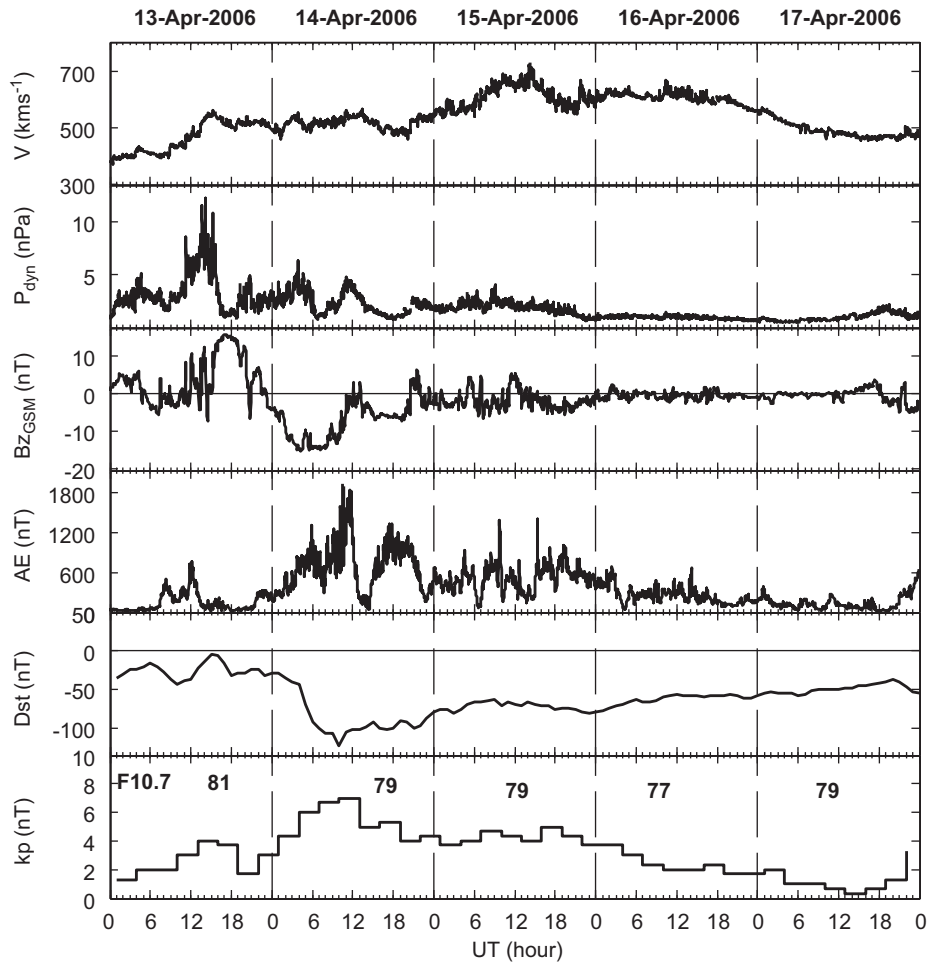

Fig. 1. Variations of solar wind parameters and geomagnetic indices during 13–17 April, 2006. From top to bottom is the solar wind velocity V_{sw}, solar wind dynamic pressure P_{dyn}, interplanetary magnetic field B_z component, AE, Dst and Kp index. The F10.7 was labeled in the Kp panel.

shown at station KO (25.5°N). Meanwhile, there was a positive storm effect at 0600 UT on 15 April at station LM (32.5°S) but negative storm effect at middle–low latitudes of the Northern Hemisphere.

We show contour maps of TEC and dTEC (by subtracting the monthly median) in Fig. 3 (subtract the monthly median) versus latitude and universal time. The top panel shows the Dst and AE indices. The middle panel illustrates the strength of the EEJ denoted by ΔH (difference between the H horizontal component at equator station CEB and non-equator station MUT). The strength of the daytime EEJ was shown to be much depressed on 13 and 16 April and hence the EIA was weak resulting in negative phase at the crest regions. In fact ΔH shows a large day-to-day variability during the month even under geomagnetic quiet condition. This could be caused by the mechanisms other than magnetic storm for example the tides variation in the lower atmosphere. During the main phase of the storm on 14 April, the DTEC at middle–low latitude zone was dominated by a strong positive storm effect with maximum value of ~30 TEC. The center of the positive phase shown at 30°N and 20°S has shifted to 20°N and 10°S after 1000 UT. The post-sunset EIA shown in TEC, usually very weak, was intensified significantly on 14 April. During the recovery phase of the storm on 15 April at 0000–0800 UT, the southern crest of EIA was shown to be much more pronounced than the northern one with maximum value around 0500–0600 UT. This is consistent with increased foF2 observed at LM as shown in Fig. 2b.

4.2. Fluctuations in hmF2 and foF2 on 14 April

As described in Section 4.1, the ionosphere at middle–low latitudes was characterized by a large positive storm effect during the main phase of the storm. To investigate how this positive storm effect was produced, we plot the evolution of hmF2 and foF2 from 4 ionosondes distributed from middle–low latitude to the equatorial area as shown in Fig. 4. The parameter hmF2 at station OS (27.3°N), CL (15.0°N), HA (8.1°N), KW (3.3°N), and LM (32.5°S) was obtained by scaling the ionograms using the SAO-explorer software (http://ulcar.uml.edu) (Reinisch et al., 2005). Three large increases in hmF2 were observed at

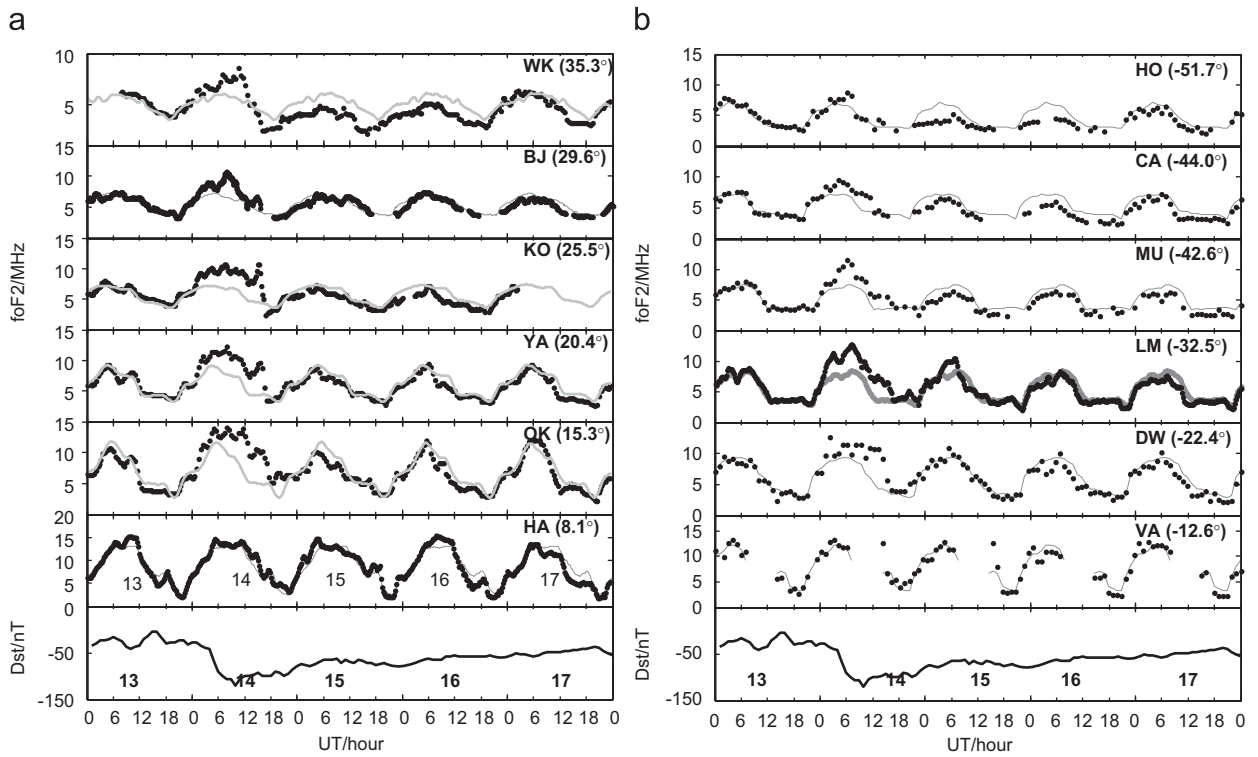

Fig. 2. The variations of foF2 during the period 13–17 April 2006 observed in the East-Asian region (a) and Australian region (b). The bottom is Dst index. Station code was labeled on the plot. In the bracket is the geomagnetic latitude of station.

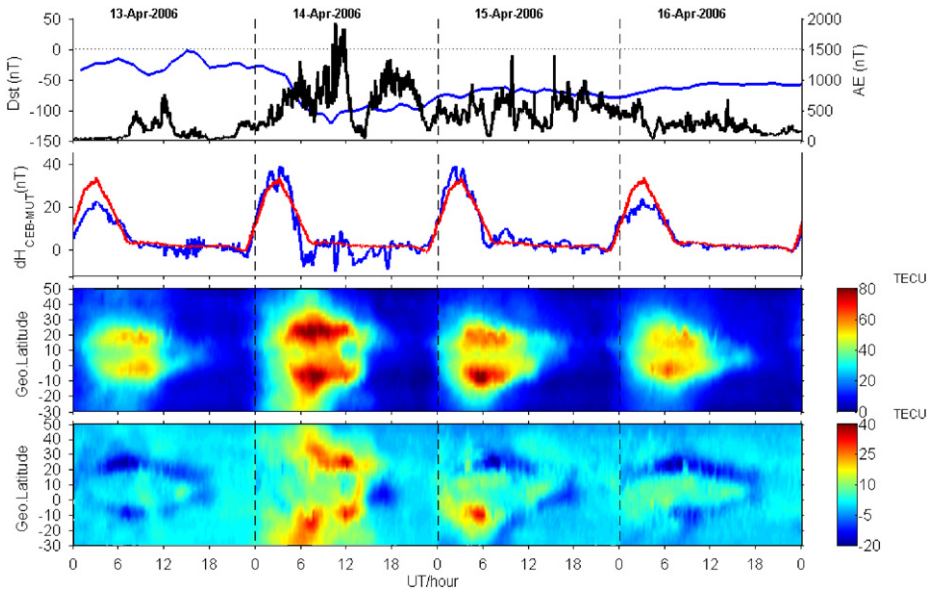

Fig. 3. From top to bottom are Dst and AE indices, ΔH (difference between the H horizontal component at equator station CEB and non-equator station MUT), contour map of TEC and DTEC vs. geographic latitude and universal time. The red line in ΔH denotes the monthly median value.

northern middle–low latitude stations OS and CL before the sunset at 1000 UT on 14 April. In contrast, there were two major height increases observed at southern middle–low latitude station LM before 0700 UT on 14 April. Meanwhile, the foF2 also shows three large increases but with an hour delay at OS and CL. The observations agree with one of the TAD characteristics that the negative initial correlation between NmF2 and hmF2 simultaneously appears in the observations and model (e.g. Bauske and Prölss, 1997; Lee et al., 2004). TAD

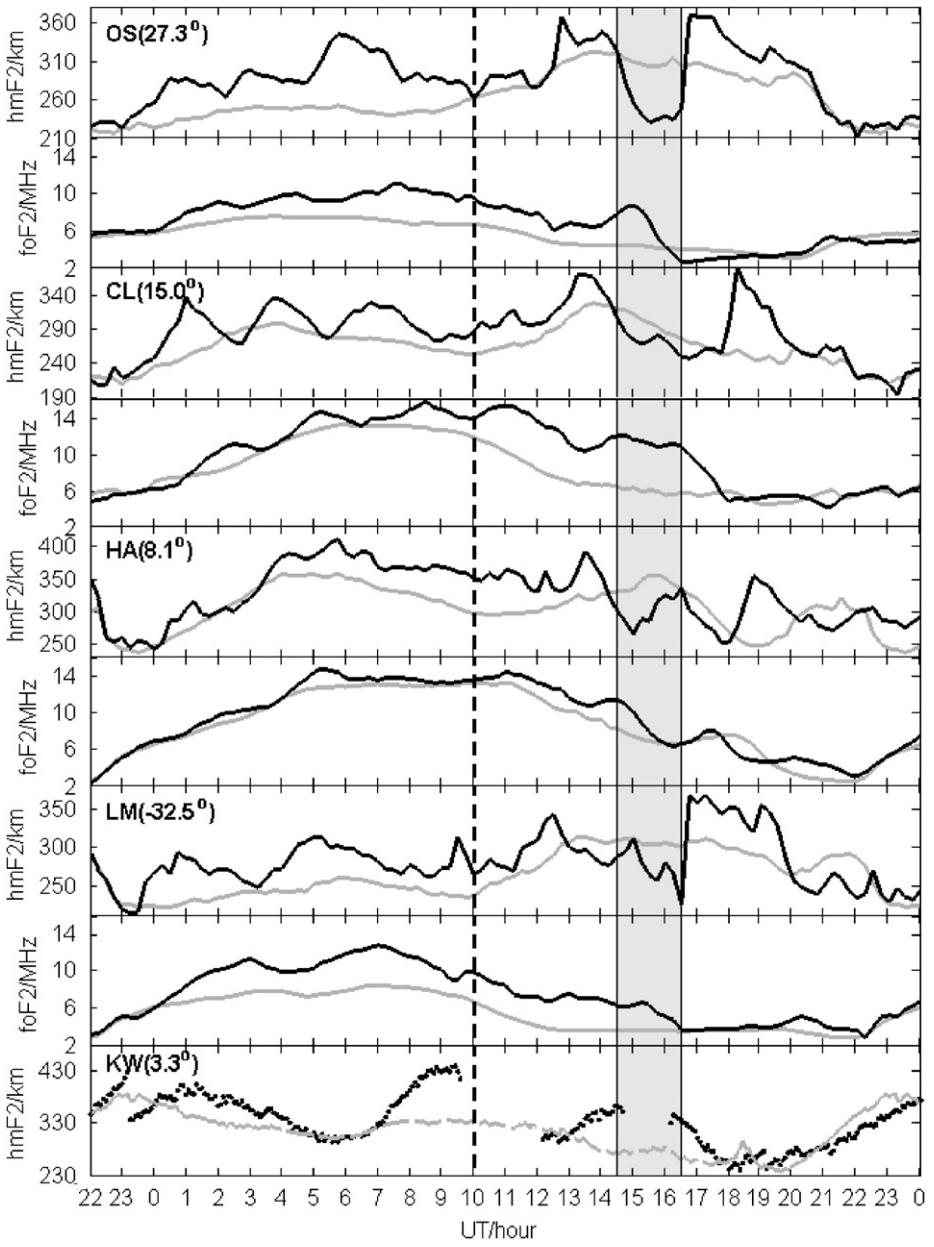

Fig. 4. foF2 and hmF2 variations at station OS, CL, HA, LM and KW from 2200 UT on 13 to 2400 UT on 14 April 2006. The gray lines represent the monthly median value. The vertical dashed line denotes the local sunset (not for KW). The gray vertical bar denotes the interval when simultaneous decreases of hmF2 were observed at middle–low latitudes.

takes the form of traveling ionospheric disturbance (TID), which can be identified from ionospheric sounding techniques and multipoint GPS network (Hajkowicz, 1990; Afraimovich et al., 1998). The TID with a horizontal scale of more than 1000 km are often referred as large-scale TID (LSTID), which propagate predominantly equatorward with a phase speed of 400–1000 m/s at East-Asian area (e.g. Tsugawa et al., 2004). From time delay of the peak and rising time of the hmF2 and the distance of OS and CL, we can estimate the phase velocity of TAD/TID in the East-Asian region. For the above three disturbances, the time delay is 30–45, 45–60, and 45–60 min. Considering the distance between two stations is about 1450 km, we can obtain phase velocity of 537–805, 402–537, and 402–537 m/s, respectively, which in the range of the previous value of propagation phase velocity for TAD/TID (Prölss, 1993). It should be noted that the obtained velocity values are quite approximate because 15-min vertical sounding data were used in the calculations. The increases in hmF2 at sub-equatorial station HA were not as regular as that observed at OS and CL. The first notable increase of hmF2 at HA appeared at ~0015 UT on 14 April. At equatorial station KW, the hmF2 was shown to increase with maximum value ~50 km

compared with reference value from 0030 to 0400 UT on 14 April associated with a large southward component of IMF B_z. However, no constant increase of hmF2 was observed at HA during this period. The ΔH component of CEB and MUT witnessed no large increase during this period as shown in Fig. 3. It is unclear that why there was different response in hmF2 at HA and KW. Perhaps the local time dependence of the penetration electric field as well as their ionospheric response should be considered because the two stations were separated ~58.2° nearly 4 h difference in the local time.

As illustrated in Fig. 4, from 0300 to 1200 UT, the hmF2 at HA showed a continuous increase superimposed with small fluctuations different from that at OS and CL. From 0800 to 1000 UT, hmF2 kept a 50 km increase at HA larger than those at OS and CL. Meanwhile, large height increase in hmF2 with maximum magnitude ~100 km occurred at KW. From 1000 to 1200 UT, there is a data gap in hmF2 at KW due to the strong spread F. At the same time hmF2 is 60 km above the reference value at HA larger than that at CL and OS. The foF2 during this period increased significantly with maximum value about 6 MHz appearing at CL. At 1230 UT on 14 April, hmF2 started a sudden uplifting about 60 km at OS. This was also observed at CL and HA with ~30–45 min delay from time delay of the peak of the hmF2 which should be caused by a TAD. The estimated phase propagating velocity was 711 m/s. A very interesting phenomenon is that hmF2 at all the three stations abruptly turned to decrease during 1430–1630 UT as denoted by vertical gray bar. This decrease can be also observed at southern station LM. Meanwhile, at equatorial station KW, hmF2 experienced a large elevation in the post-midnight sector indicating an existence of large eastward-disturbed electric field. The anticorrelation between the equatorial and middle–low latitude F-layer height disturbances resembles the "mirroring" effect, which was described by Rishbeth et al. (1978) on the basis of incoherent scatter radar observations. The foF2 was shown to be greatly enhanced during this period at northern middle latitude as shown in Fig. 2a, and this should be caused by the enhanced fountain effect due to an eastward-disturbed electric field. The sudden decrease of hmF2 was terminated by a large elevation at higher latitude station OS and LM around 1645 UT. However, this large post-midnight height disturbance was observed to start 75–90 min later at CL and HA. From time delay of the rising time of the increased hmF2 between OS and CL, the phase propagation of TAD/TID is ~289 m/s, which is much less than the normal value of TAD/TID at night (Prölss, 1993). From time delay of the rising time of the increased hmF2 between CL and HA, the phase propagation of TAD/TID is ~778 m/s. The inconsistency for the height

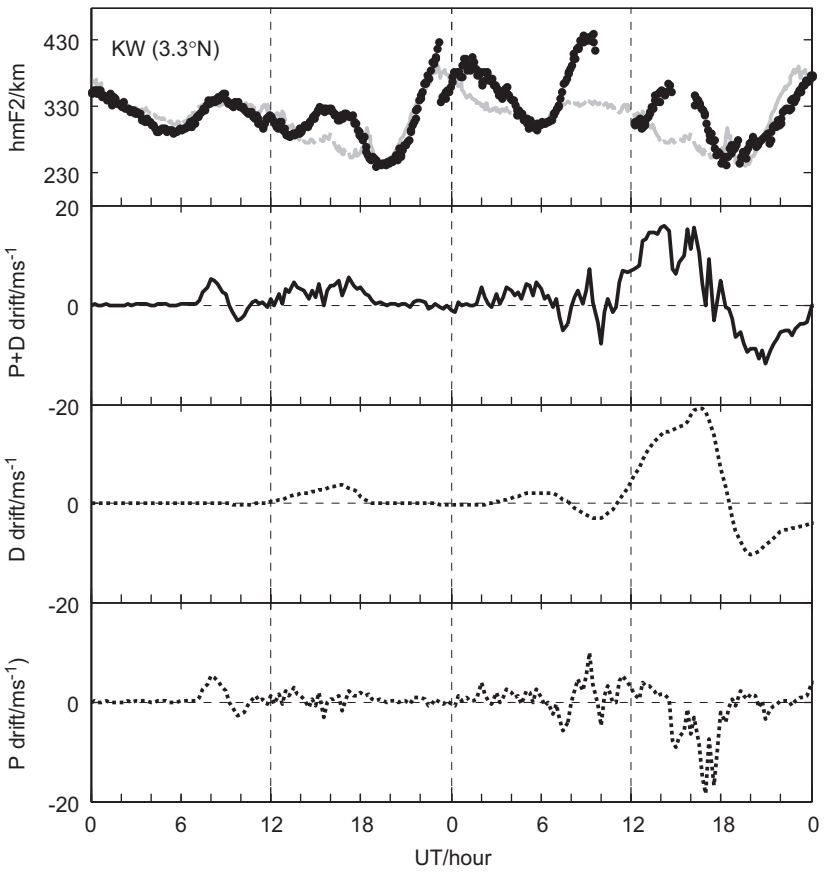

Fig. 5. From top to bottom is the hmF2 at equatorial station KW (gray line is the reference value), disturbed equatorial vertical drift, disturbed vertical drift caused by wind disturbance dynamo electric field and by penetration electric field on 14 April 2006.

disturbances at three stations shows that the plasma movement at middle–low latitudes at this time was complicated and may not necessarily link to TAD/TID. As shown in Fig. 3 that there was depletion in the equatorial TEC during 1500–1800 UT suggesting an existence of an eastward disturbance dynamo electric field. A downward component along the magnetic field could possibly offset the upward component due to the equatorward TAD inducing delay response of hmF2 at HA and CL with respect to the OS. The detailed mechanism causing this difference needs further study.

4.3. *Prompt penetration electric field and disturbance dynamo electric field effects at West Pacific area*

Two broad types of disturbance electric fields could severely affect the equatorial ionosphere during the storms or substorms event: (a) direct penetration of magnetospheric electric fields, involving hydromagnetic wave propagation as in the storm sudden commencement phase (Kikuchi, 1986) or substorm current system and shielding charges in the inner boundary of the magnetosphere as in substorm development and recovery phases associated with southward/ northward IMF polarity changes (e.g. Kelley et al., 1979; Fejer et al., 1979; Gonzales et al., 1979; Spiro et al., 1988). (b) Disturbance dynamo electric field produced by the disturbed thermospheric circulation and neutral winds originating from storm energy deposition in the high latitude thermosphere (Blanc and Richmond, 1980). By binning Jicamarca (11.9°S, 76.8°W, dip °2) vertical $E \times B$ plasma drift data according to local time and the time from major perturbations in the geomagnetic AE index, Fejer and Scherliess (1997) developed an empirical model to determine the piecewise linear relationship between the disturbance electric fields and AE values, which separated the effects of the prompt penetration electric field from those of the disturbance dynamo electric field.

In this case, both effects has been clearly identified by hmF2 variation at equatorial station KW (167.2°E, 3.3°N, LT = UT+11) as shown in Fig. 5. The top panel illustrates the hmF2 variation during 13–14 April 2006 and the gray line is for the value of the quiet time median. The bottom three panels are storm-time vertical drifts in the equatorial zone at longitude 167.2°E calculated from the model of Fejer and Scherliess (1997). The broken and solid lines represent the drifts being produced by the disturbance dynamo electric field, the prompt penetration electric field, and both, respectively. Comparing with the height evolution at KW, the model showed its good prediction ability for disturbance dynamo electric fields than penetration electric fields. The model predicted a large upward drift during the period 1200–1800 UT for both the day 13 and 14 April though the former one was underestimated. The model also predicted an upward drift being produced by the penetration electric field during 0700–0800 UT on 14 April, while IMF B_z was southward and AE experienced a sudden increase. The model predicted an upward drift during 0700–0900 UT on 13 April, which should be attributed to the increased auroral activity during this period as the model was built on the basis of AE index. However, no evident enhancement in hmF2 was observed at KW. The model predicts small upward drift during 0200–0500 UT on 14 April with an hour delay to the observed increased hmF2 variation.

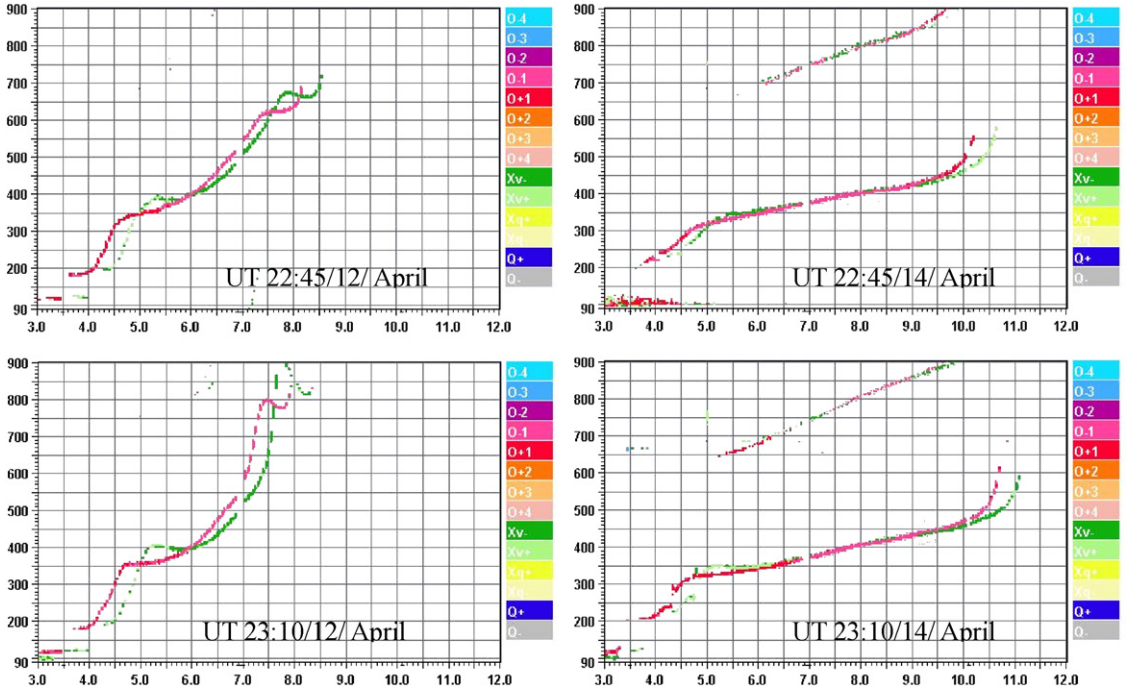

Fig. 6. Ionograms shown at 2245 and 2310 UT on 12 (left) and 14 April (right).

These inconsistencies might be due to the fact that the model corresponds to the average conditions of the Jicamarca drift database and is limited by crude parameterization of the Joule heating at high latitudes and day-to-day variability of the quiet time atmospheric dynamo electric fields (Scherliess and Fejer, 1997). In addition, the photochemistry of the daytime could mask the hmF2 response to disturbance electric fields leading to the discrepancy between the observed hmF2 and predicted upward drift.

The model also shows that during 2000–2400 UT on 14 April there was a westward disturbance dynamo electric field. The hmF2 at KW was shown to be depressed 30 km in the morning–noon sector than the reference value. An interesting phenomenon is that F3-layer was inhibited during this time comparing with the quiet day which can be identified from the ionograms. Normally, the F3-layer is an additional layer that usually forms during the morning–noon period at altitudes above the F2-layer peak; its peak density usually can exceed the peak density of the F2-layer and it arises from the vertical $E \times B$ drift at the geomagnetic equator and is modulated by neutral wind (Balan et al., 1997). Evidence was shown that the peak height of the F2-layer undergoes a rapid decrease if the peak height of the F-layer changes from the F3-layer to the F2-layer (Paznukhov et al., 2007). This is the reason why hmF2 fell quickly from 2200 to 2400 UT on 13 April as indicated in Fig. 5.

Fig. 6 shows a comparison of the ionograms at 2245 and 2310 UT on 12 and 14 April. The F3-layer at station KW for the quiet day of April appears for a short period of time just before noon (2200–2330 UT). However, the F3-layer disappeared on 14 April during the same period and foF2 increased from 8 to 10 MHz. This positive storm effect could be possibly caused by several processes. First, if the storm equatorward wind occurred simultaneously in both hemispheres ionization would build up at the equator due to the wind convergence effect (Fesen et al., 1989). Second, the downwelling of the atmosphere causes a decrease in molecular gases in the thermosphere, leading to a decrease of recombination rate of O^+, and then induce a positive storm effect (Rishbeth et al., 1987). Furthermore, this enhancement can also caused by a reduced fountain effect that is caused by westward electric field. Model calculations are required to specify the quantitative contribution of electric field and wind or other factors to the inhabitation of F3-layer which is beyond the scope of this paper.

4.4. Thermospheric response

The orbit of GUVI observation has 74.1° inclination with a 97.8 min period. The orbital precession rate is such that the beta angle (the angle between the Earth–Sun vector and the orbital plane) passes through zero every 120 days, so the local time of the orbit varies with this periodicity. As a consequence, GUVI samples all local solar times every 60 days, counting ascending and descending node orbits. The local time distribution varies a little when pass the same region in consecutive several days. The estimated errors in O/N_2 might reach 10% for high O/N_2 values and latitudes above 60° but are expected to be close to 5% for low O/N_2 values and at lower latitudes. Although some questions about absolute O/N_2 values still need to be resolved due to uncertainties in cross sections, relative variations in O/N_2 ratio should not be affected, as discussed by Christensen (2003) and Strickland et al. (2004). Fig. 7 presents the GUVI [O/N_2] distribution with equatorial local time sector 0630 LT during 12–18 April 2006 in the East-Asian/Australian region. The mean universal time of every orbit passing the area was labeled on the map. It is shown that the reduced O/N_2 region expanded to the geographic latitudes 45°N around 2030 UT and 40°S around 2230 UT on 13 April. The negative phase of O/N_2 is most significant on 14 and 15 April as it reached geographic latitude 35°N and 30°S and became diminished on 16 April. This agrees well with the

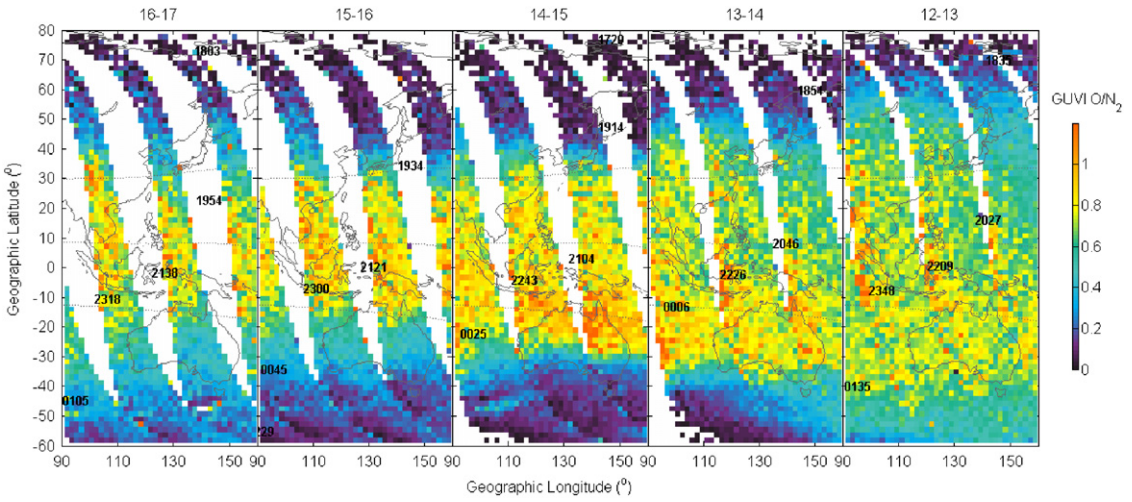

Fig. 7. GUVI O/N_2 ratio during 12–17 April 2006. The data were recorded around 0630 LT at equator for the longitudes 90–160°E. The centered universal time, mean value of each orbit, was labeled as black text. The thin dashed line represents the dip inclination 0° and ±30°.

fact that negative phase in foF2 reach to lower geomagnetic latitudes in the Northern Hemisphere than in the Southern Hemisphere as displayed in Fig. 2. In the low latitudes, due to a Hadley-type circulation cell that produces its convergence and downwelling in the low and middle latitudes (Rishbeth et al., 1987), O/N_2 increased from 0.8 to 1.2 with largest value appearing at 20–30°S in the Australia on 14 April around 2100 UT. This may contribute some to the positive phase of the foF2 observed in the low and equatorial latitudes.

5. Discussion

In this paper, we reported ionospheric storm effects during the magnetic storm for period 13–17 April 2006. The storm is characterized by a large long-duration positive storm effect superimposed with wave structure in foF2 and hmF2 from middle to low latitudes during the main phase of the storm. The feature is quite similar to that observed in foF2 and hmF2 during the daytime at East-Asian area discovered by Pirog et al. (2007) during the intense storm 7–10 November 2004. Their results show that LSTIDs propagated predominantly southwestward at mean velocities of 200 and 400 m/s on 8 and 10 November. The long-duration positive storm effect at middle–low latitudes for the present case can be attributed to several mechanisms. During the period 0000–0600 UT, the periodic enhancement of foF2 should be caused by the storm-time equatorward wind superimposed with TADs. As shown in Fig. 1, AE began to increase at 2130 UT on 13 April, and hmF2 was observed first to be elevated around 2300 and 2330 UT at middle–low latitude station OS and LM for both the hemispheres. One would think that the increase of AE is small that it cannot account for the large rapid response of the ionosphere at middle–low latitudes. However, in the low solar activity and at pre-dawn sector, both the density of neutral particles and plasma density are reduced and correspondingly decreases the damping rate of the LSTIDs (Hajkowicz, 1990). Since gravity wave excitation is dependent on the spatial and temporal source properties, excitation of large-scale gravity waves occurs even under low geomagnetic conditions with relatively low energy depositions but optimal source properties (Mayr et al., 1990). In addition, Haijkowicz (1995) also revealed that morning virtual height enhancement of ionospheric F-layer (h′F) after the onset of auroral substorm activity is a prominent feature of the disturbed ionosphere. He proposed that this large morning height enhancement would be constructive interference between large-scale waves generated by the auroral source and by the supersonic motion of the sunrise terminator.

Recent studies showed that the penetration electric fields from magnetospheric origin could be important to explain the positive storm effects during the early stage of storms before the full development of storm-induced winds and the generated disturbance neutral wind dynamo (Huang et al., 2005). During the period 0000–0600 UT on 14 April, IMF B_z was shown to be southward turning associated with an increased auroral activity. The magnetospheric convection electric field may penetrate to the equatorial ionosphere producing the increased hmF2 during 0000–0400 UT at KW. Meanwhile, there was an increment in hmF2 at 0100 and 0400 UT at HA which is 60° westward of the KW. Since the magnetic dip inclination of HA is 26.8°, this height disturbance may be caused by both the electric field and equatorward wind. The strength of the EEJ denoted by ΔH in the daytime can be a good indicator of the existence of strong disturbed electric field (Anderson et al., 2002). Usually ΔH shows a large spiky increase if there is a strong magnetospheric electric field penetrated to the equator. This situation has also been observed during the events investigated by Huang et al. (2005) using the magnetometer at Jicamarca (http://jro.igp.gob.pe). For the present case, EEJ shows no evident large intensification as illustrated in Fig. 3. We are lack of observational proof of large electric field in the East-Asian region. Considering the equatorward winds have a component along the magnetic field lines in the opposite direction to field-aligned diffusion limiting the development of EIA (e.g. Lei et al., 2007), the electric field may also play an important role in causing the positive storm effect during the morning–noon sector. The wave-like structure during the morning–noon sector was observed in the East-Asian region during the magnetic storm 6–8 April 2000 (Lee et al., 2004) and is common during the magnetic storm in the East-Asian region. Lei et al. (2008b) successfully reproduced the daytime wave structure in NmF2 at East-Asian area using CMIT 2.0 model. Their term analysis of the ion continuity equation demonstrated that the ionospheric oscillations in this event were mainly induced by the disturbed neutral winds superimposed with TAD although the electric field made some contribution. We have investigated scores of ionospheric storm effects in the East-Asian region and found quite a few were characterized by this consecutive wave-like structure. The statistical results will be given in another paper.

From 0400 to 1400 UT, the hmF2 at HA showed a continuous enhancement with amplitudes being larger than that at OS and CL after 0700 UT. Meanwhile, there was a large increase in hmF2 observed at KW during 0700–1000 UT. The positive phase in foF2 especially at night during this period would be most probably caused by both the equatorward wind and an eastward penetration electric field, although it is shown from the GUVI data that O/N_2 increased during the storm at middle–low latitudes in this longitude. Model simulations of Lin et al. (2005) shows that combined effects of upward $E \times B$ drift and meridional winds produce the most significant plasma enhancement at low latitude. If meridional winds blow equatorward, the ion drag along magnetic field lines will oppose the downward diffusion and keep the plasma at altitudes where the recombination rate is lower. As a result, the peak density will increase significantly and also its position will shift to higher latitudes. Lei et al. (2008a) have investigated the thermospheric and ionospheric response during the initial phase of the magnetic storm on 14–15 December 2006 using a Coupled Magnetosphere Ionosphere Thermosphere (CMIT) 2.0 model simulation. Term analysis of the ion continuity equation demonstrates

that changes in the electric fields play a dominant role in generating the observed ionospheric positive storm effect in the American sector during the initial phase, although neutral winds and composition changes also contribute. Model simulation is needed to explore the relative importance of the winds, electric fields and composition in explaining the large-scale storm effects for the present case which will be considered in our further study.

Another feature of the ionospheric response in this region was that the positive storm effect became more pronounced at crest region in the Southern Hemisphere during 0000–0600 UT on 15 April as illustrated in Fig. 3. The negative phase appeared at lower geomagnetic latitudes in the Northern Hemisphere than in the Southern Hemisphere on 15 April. The ionospheric response shows a clear hemispheric asymmetry with respect to the geomagnetic equator. This is also indicated by the GUVI O/N_2 shown in Fig. 7 that the value was smaller and reached to lower geomagnetic latitudes in the Northern Hemisphere at the East-Asian longitude on 14–15 April. Also O/N_2 increased with largest value appearing at 20–30°S in the Australia. Thus a southward wind transports plasma horizontally from the northern EIA crest across the equator and into the southern crest could possibly explained the southern positive storm effect (Fesen et al., 1989). Another mechanism that induces the hemispheric asymmetry of the positive storm effects was proposed by Lei et al. (2008a) to be attributed to the differences of the slope (or scale height) of the lower topside electron density profile. The elevation of hmF2 could result in more increased foF2 due to the smaller scale height in the Southern Hemisphere at middle–low latitudes on 15 April. The change in scale heights is caused by the higher plasma temperatures in the summer hemisphere and the neutral circulation from the summer to the winter hemisphere. It was shown from GUVI O/N_2 data that the O/N_2 distribution asymmetry at high–middle latitude for the two hemispheres was large on 12 April.

From 1400 to 1700 UT of 14 April in the nighttime, the large enhancement of foF2 should result from the effect of wind-disturbed dynamo electric field as shown in Fig. 5. We notice that at 1400–1600 UT on 14 April, hmF2 shows abruptly drop, especially at higher latitude station OS, at all the middle–low latitudes stations associated with a large increase of hmF2 at equatorial station KW. The anticorrelation between the hmF2 at equatorial and middle–low latitudes could possibly attributed to the anticorrelation between $V_{\parallel}$ and $V_{\perp}$, the components of F2-layer plasma velocity parallel to and perpendicular to the geomagnetic field. This was termed as 'mirroring' effect (Behnke and Harper, 1973), which has been theoretically studied by Rishbeth et al. (1978). When a strong eastward electric field produces a strong equatorial plasma fountain, the plasma will move upward and poleward to field lines with higher magnetic inclination, where downward diffusion is faster (Lin et al., 2005). Stronger field-aligned ion flows, due to the mirror effect tends to cancel out the possible lift of the peak height of the F2-layer at low latitudes due to eastward electric field, resulting nearly horizontal motion or even decrease of the height of the F-layer. Note that this mirror effect only operates on middle–low latitudes, and becomes ineffective with decreasing dip angle. Detailed mechanism of this sudden decreased hmF2 still needs further investigation.

6. Conclusion

In this paper, we have analyzed the ionospheric storm effect based on the ionosonde chain and GPS network and space-based GUVI data at west Pacific area during the intense geomagnetic storm on 13–17 April 2006. From the view point of large-scale variation, the storm produced prominent positive ionospheric storm effect for both the Northern and Southern Hemispheres during the initial and main phase of the storm on 14 April in the middle to low latitudes. During the recovery phase, negative storm effect was shown to permeate to the middle–low latitudes and persisted for 2–3 days, which was due to the reduced O/N_2 according to the observation of GUVI. Both the positive storm and negative storm effect presented a seasonal effect of the ionospheric storm which should be attributed to the background thermospheric condition 20 days after the vernal equinox. Periodic wave structures of foF2 at middle–low latitudes in the morning sector on 14 April should be caused by TADs with phase propagation velocities ranging 400–800 m/s, while in the afternoon and nighttime, the positive phase would be most probably caused by both the enhanced equatorward winds and disturbed eastward electric fields. The model of Fejer and Scherliess (1997) shows its good prediction ability for the disturbance dynamo electric field than penetration electric field comparing with the variation of equatorial hmF2.

Acknowledgments

This research was supported by National Natural Science Foundation of China (40804041, 40725014) and National Important Basic Research Project (2006CB806306). The authors acknowledge IGS for providing the GPS data in the web site. Special thanks should be given to Prof. B. Reinisch for offering the DIDB database and Ionospheric Prediction Service of Australia for providing data in Australia. The equatorial Dst data were obtained from World Data Center C2 for Geomagnetism in Kyoto. We also thank the Dr. A.B. Christensen and L. Paxton, the PI and Project Scientist of the GUVI team for providing $[O/N_2]$ data.

References

Abdu, M.A., 1997. Major phenomena of the equatorial ionosphere–thermosphere system under disturbed conditions. Journal of Atmospheric and Solar-Terrestrial Physics 13, 1505–1519.

Abdu, M.A., Sobral, J.H.A., Paula, E.R., Batista, I.S., 1991. Magnetospheric disturbance effects on the Equatorial Ionization Anomaly (EIA): an overview. Journal of Atmospheric and Solar-Terrestrial Physics 53, 757–771.

Afraimovich, E.L., Palamartchouk, K.S., Perevalova, N.P., 1998. GPS radio interferometry of travelling ionospheric disturbances. Journal of Atmospheric Solar-Terrestrial Physics 60, 1205–1223.

Anderson, D., Anghel, A., Yumoto, K., Ishitsuka, M., Kudeki, E., 2002. Estimating daytime vertical $E \times B$ drift velocities in the equatorial F-region using ground-based magnetometer observations. Geophysical Research Letters 29 (12), 1596.

Balan, N., Bailey, G.J., Abdu, M.A., Oyama, K.I., Richards, P.G., MacDougall, J., Batista, I.S., 1997. Equatorial plasma fountain and its effects over three locations: evidence for an additional layer, the F3 layer. Journal of Geophysical Research 102, 2047–2056.

Bauske, R., Prölss, G.W., 1997. Modeling the ionospheric response to traveling atmospheric disturbances. Journal of Geophysical Research 102, 14,555–14,562.

Behnke, R.A., Harper, R.M., 1973. Vector measurements of F region ion transport at Arecibo. Journal of Geophysical Research 78, 8222.

Blanc, M., Richmond, A.D., 1980. The ionospheric disturbance dynamo. Journal of Geophysical Research 85, 1669–1686.

Buonsanto, M.J., 1999. Ionospheric storms—a review. Space Science Reviews 88, 563–601.

Burns, A.G., Killeen, T.L., Carignan, G.R., Roble, R.G., 1995. Large enhancements in the O/N_2 ratio in the evening sector of the winter hemisphere during geomagnetic storms. Journal of Geophysical Research 100, 14,661–14,671.

Burns, A.G., Solomon, S.C., Wang, W., Killeen, T.L., 2007. The ionospheric and thermospheric response to CMEs: challenges and successes. Journal of Atmosphere and Solar-Terrestrial Physics 69, 77–85.

Christensen, A.B., 2003. Initial observations with the global ultraviolet imager (GUVI) in the NASATIMED satellite mission. Journal of Geophysical Research 108 (A12), 1451.

Danilov, A.D., Lastovička, J., 2001. Effects of geomagnetic storms on the ionosphere and atmosphere. International Journal of Geomagnetism and Aeronomy 2, 209–224.

Fejer, B.G., Scherliess, L., 1997. Empirical models of storm time equatorial electric fields. Journal of Geophysical Research 102, 24,047–24,056.

Fejer, B.G., Gonzalez, C.A., Farley, D.T., Kelly, M.C., 1979. Equatorial electric fields during magnetically disturbed conditions, 1, The effect of the interplanetary magnetic field. Journal of Geophysical Research 84, 5797–5802.

Fesen, C.G., Growley, G., Roble, R.G., 1989. Ionospheric effects at low latitudes during the March 22, 1979, geomagnetic storm. Journal of Geophysical Research 94, 5405–5417.

Fuller-Rowell, T.J., Codrescu, M.V., Moffett, R.J., Quegan, S., 1994. Response of the thermosphere and ionosphere to geomagnetic storms. Journal of Geophysical Research 99, 3893–3914.

Fuller-Rowell, T.J., Codrescu, M.V., Rishbeth, M.V., Moffett, R.J., Quegan, S., 1996. On the seasonal response of the thermosphere and ionosphere to geomagnetic storms. Journal of Geophysical Research 101, 2343–2353.

Gonzales, C.A., Kelley, M.C., Fejer, B.G., Vickrey, J.F., Woodman, R.F., 1979. Equatorial electric fields during magnetically disturbed conditions, 2, Implications of simultaneous auroral and equatorial measurements. Journal of Geophysical Research 84, 5803–5812.

Hajkowicz, L.A., 1990. A global study of large-scale traveling ionospheric disturbances (TIDs) following a step-like onset of auroral substorms in both hemispheres. Planetary Space Science 38, 913–923.

Haijkowicz, L.A., 1995. Ionospheric response to auroral substorms during sunspot maximum (1980–82). Annales Geophysics 25 (13), 95–104.

Huang, C.-S., Foster, J.C., Goncharenko, L.P., Erickson, P.J., Rideout, W., Coster, A.J., 2005. A strong positive phase of ionospheric storms observed by the Millstone Hill incoherent scatter radar and global GPS network. Journal of Geophysical Research 110, A06303.

Immel, T.J., Crowley, G., Craven, J.D., Roble, R.G., 2001. Dayside enhancements of thermospheric O/N_2 following magnetic storm onset. Journal of Geophysical Research 106, 15,471–15,488.

Kane, R.P., 2005. Ionospheric foF2 anomalies during some intense geomagnetic storms. Annales Geophysics 23, 2487–2499.

Kelley, M.C., Fejer, B.G., Gonzales, C.A., 1979. An explanation for anomalous equatorial ionospheric electric fields associated with a northward turning of the interplanetary magnetic field. Geophysical Research Letters 6, 301–304.

Kikuchi, T., 1986. Evidence of transmission of polar electric fields to the low latitude at times of geomagnetic sudden commencements. Journal of Geophysical Research 91, 3101–3105.

Kutiev, I., Watanabe, S., Otsuka, Y., Saito, A., 2005. Total electron content behavior over Japan during geomagnetic storms. Journal of Geophysical Research 110, A01308.

Lee, C.-C., Liu, J.-Y., Chen, M.-Q., Su, S.-Y., Yeh, H.-C., Nozaki, K., 2004. Observation and model comparisons of the traveling atmospheric disturbances over the Western Pacific region during the 6–7 April 2000 magnetic storm. Journal of Geophysical Research 109, A09309.

Lei, J., et al., 2007. Comparison of COSMIC ionospheric measurements with ground-based observations and model predictions: preliminary results. Journal of Geophysical Research 112, A07308.

Lei, J., Wang, W., Burns, A.G., Solomon, S.C., Richmond, A.D., Wiltberger, M., Goncharenko, L.P., Coster, A., Reinisch, B.W., 2008a. Observations and simulations of the ionospheric and thermospheric response to the December 2006 geomagnetic storm: initial phase. Journal of Geophysical Research 113, A01314.

Lei, J., Burns, A.G., Tsugawa, T., Wang, W., Solomon, S.C., Wiltberger, M., 2008b. Observations and simulations of quasiperiodic ionospheric oscillations and large-scale traveling ionospheric disturbances during the December 2006 geomagnetic storm. Journal of Geophysical Research 113, A06310.

Lekshmi, D.V., Balan, N., Vaidyan, V.K., Alleyne, H., Bailey, G.J., 2008. Response of the ionosphere to super geomagnetic storms: observations and modeling. Advances in Space Research 41, 548–555.

Lin, C.H., Richmond, A.D., Heelis, R.A., Bailey, G.J., Lu, G., Liu, J.Y., Yeh, H.C., Su, S.-Y., 2005. Theoretical study of the low- and midlatitude ionospheric electron density enhancement during the October 2003 superstorm: relative importance of the neutral wind and the electric field. Journal of Geophysical Research 110, A12312.

Liu, L., Wan, W., Lee, C.C., Ning, B., Liu, J.Y., 2004. The low latitude ionospheric effects of the April 2000 magnetic storm near 120°E. Earth Planets Space 56, 607–612.

Lynn, K.J.W., Sjarifudin, M., Harris, T.J., Le Huy, M., 2004. Combined TOPEX/Poseidon TEC and ionosonde observations of negative low-latitude ionospheric storms. Annales Geophysics 22, 2837–2847.

Mannucci, A.J., Tsurutani, B.T., Iijima, B.A., Komjathy, A., Saito, A., Gonzalez, W.D., Guarnieri, F.L., Kozyra, J.U., Skoug., R., 2005. Dayside global ionospheric response to the major interplanetary events of October 29–30, 2003 "Halloween Storms". Geophysical Research Letters 32, L12S02.

Mao, T., Wan, W., Yue, X., Sun, L., Zhao, B., Guo, J., 2008. An empirical orthogonal function model of total electron content over China. Radio Science 43, RS2009.

Maruyama, T., Nakamura, M., 2007. Conditions for intense ionospheric storms expanding to lower midlatitudes. Journal of Geophysical Research 112, A05310.

Mayr, H.G., Harris, I., Herrero, F.A., Spencer, N.W., Varosi, F., Pesnell, W.D., 1990. Thermospheric gravity waves: observations and interpretation using the transfer function model (TFM). Space Science Reviews 54, 297–375.

Meier, R., Crowley, G., Strickland, D.J., Christensen, A.B., Paxton, L.J., Morrison, D., Hackert, C.L., 2005. First look at the 20 November 2003 superstorm with TIMED/GUVI: comparisons with a thermospheric global circulation model. Journal of Geophysical Research 110, A09S41.

Mendillo, M., 2006. Storms in the ionosphere: patterns and processes for total electron content. Reviews of Geophysics 44, RG4001.

Paxton, L.J., 2004. GUVI: a hyperspectral imager for geospace. In: Instruments, Science, and Methods for Geospace and Planetary Remote Sensing, Proceedings of SPIE, vol. 5660. SPIE, Bellingham, WA, pp. 227–240.

Paznukhov, V.V., Reinisch, B.W., Song, P., Huang, X., Bullett, T.W., Veliz, O., 2007. Formation of an F3 layer in the equatorial ionosphere: a result from strong IMF changes. Journal of Atmospheric and Solar-Terrestrial Physics 69, 1292–1304.

Pirog, O.M., Polekh, N.M., Tashchilin, A.V., Romanova, E.B., Zherebtsov, G.A., 2006. Response of ionosphere to the great geomagnetic storm of September 1998: observation and modeling. Advances in Space Research 37, 1081–1087.

Pirog, O.M., Polekh, N.M., Voeykov, S.V., Zherebtsov, G.A., Tatarinov, P.V., 2007. Ionospheric disturbances in the East-Asian region during geomagnetic storm in November, 2004. Advances in Space Research 39, 1335–1341.

Prölss, G.W., 1993. Common origin of positive ionospheric storms at middle latitudes and the geomagnetic activity effect at low latitudes. Journal of Geophysical Research 98, 5981–5991.

Prölss, G.W., 1995. Ionospheric F-region storms. In: Volland, H. (Ed.), Handbook of Atmospheric Electrodynamics. CRC Press, Boca Raton, FL.

Scherliess, L., Fejer, B.G., 1997. Storm time dependence of equatorial disturbance dynamo zonal electric fields. Journal of Geophysical Research 102, 24,037–24,046.

Reinisch, B.W., Huang, X., Galkin, I.A., Paznukhov, V., Kozlov, A., 2005. Recent advances in real-time analysis of ionograms and ionospheric drift measurements with digisondes. Journal of Atmospheric and Solar-Terrestrial Physics 67, 1054–1062.

Rishbeth, H., Ganguly, S., Walker, J.G.G., 1978. Field-aligned and field-perpendicular velocities in the ionospheric F2-layer. Journal of Atmospheric and Terrestrial Physics 40, 767–784.

Rishbeth, H., Fuller-Rowell, T.J., Rees, D., 1987. Diffusive equilibrium and vertical motion in the thermosphere during a sever magnetic storm: a computational study. Planetary Space Science 35, 1157–1165.

Schunk, R.W., Sojka, J.J., 1996. Ionosphere–thermosphere space weather issues. Journal of Atmospheric Solar-Terrest Physics 58, 1527–1574.

Spiro, R.W., Wolf, R.A., Fejer, B.G., 1988. Penetration of highlatitude electric-field effects to low latitudes during SUNDIAL 1984. Annales of Geophysics 6, 39–50.

Strickland, D.J., Meier, R.R., Walterscheid, R.L., Craven, J.D., Christensen, A.B., Paxton, L.J., Morrison, D., Crowley, G., 2004. Quiettime seasonal behavior of the thermosphere seen in the far ultraviolet dayglow. Journal of Geophysical Research 109, A01302.

Tsugawa, T., Saito, A., Otsuka, Y., 2004. A statistical study of largescale traveling ionospheric disturbances using the GPS network in Japan. Journal of Geophysical Research 109 (9), A06302.

Yizengaw, E., Dyson, P.L., Essex, E.A., Moldwin, M.B., 2005. Comprehensive ionosphere dynamics study over the Southern Hemisphere during the severe magnetic storm on 31 March 2001. Annales of Geophysics 23, 707–721.

Yumoto, K., the MAGDAS Group, 2006. MAGDAS project and its application for space weather. In: Gopalswamy, N., Bhattacharyya, A. (Eds.), Solar Influence on the Heliosphere and Earth's Environment: Recent Progress and Prospects, pp. 309–405.

Zhao, B., Wan, W., Liu, L., 2005. Responses of equatorial anomaly to the October–November 2003 superstorms. Annales of Geophysics 23, 693–706.

Zhao, B., Wan, W., Liu, L., Mao, T., 2007. Morphology in the total electron content under geomagnetic disturbed conditions: results from global ionosphere maps. Annales of Geophysics 25, 1555–1568.